European Journal of Pharmaceutics and Biopharmaceutics 142 (2019) 473–479

Contents lists available at ScienceDirect

European Journal of Pharmaceutics and Biopharmaceutics

journal homepage: www.elsevier.com/locate/ejpb

Research paper

RNA G-quadruplex as supramolecular carrier for cancer-selective delivery

Tiago Santos[a], Patrícia Pereira[b], Maria Paula Cabral Campello[c], António Paulo[c], João A. Queiroz[a], Eurico Cabrita[d], Carla Cruz[a,*]

[a] CICS-UBI-Centro de Investigação em Ciências da Saúde, Universidade da Beira Interior, Av. Infante D. Henrique, Covilhã 6200-506, Portugal
[b] Instituto de Tecnologia Química e Biológica António Xavier, Universidade Nova de Lisboa, Avenida da República, Oeiras 2780-157, Portugal
[c] Centro de Ciências e Tecnologias Nucleares, Instituto Superior Técnico, Universidade de Lisboa, Estrada Nacional 10 (km 139,7), Bobadela LRS 2695-066, Portugal
[d] UCIBIO, REQUIMTE, Departamento de Química, Faculdade de Ciências e Tecnologia, Universidade Nova de Lisboa, Caparica 2829-516, Portugal

ARTICLE INFO

Keywords:
Precursor microRNA 149
G-quadruplex
Nucleolin
Drug delivery
Prostate cancer

ABSTRACT

Nucleic acid aptamers have emerged as an attractive class of carrier molecules due to their ability to bind with high affinity to specific ligands; their high chemical flexibility; as well as tissue penetration capability. RNA G-quadruplex (rG4) sequences have been described as structures with high stability and selectivity towards cancer cells. Recently, precursor microRNAs (pre-miRNAs) have been described as new G4 forming molecules. Surface nucleolin (NCL) is a known target of aptamer G4 AS1411 and is overexpressed on prostate cancer cells when compared with normal cells. We have shown that the sequence 5′ GGGAGGGAGGGACGGG 3′ found in pre-miR-149 forms a rG4 parallel structure, which can bind NCL. Also, another rG4 sequence with a longer loop was evaluated in terms of G4 formation, stabilization and binding affinity to NCL.

Both rG4s sequences were studied as supramolecular carriers for the cancer-selective delivery of acridine ligand C_8. The rG4s-C_8 complexes showed high affinity ($K_D = 10^{-6}$ M) and stabilization ($T_m > 30$ °C). The affinity of the rG4s-C_8 complexes against NCL was in the low nanomolar range, indicating that C_8 did not affect NCL binding. Noteworthy, the short loop rG4-C_8 complex showed selective antiproliferative effects in prostate cancer cells when compared with normal prostatic cells. The stability and nuclease resistance of rG4 and rG4-C_8 complex were evaluated in biological conditions and revealed the maintenance of G4 structure and complex stability. Furthermore, confocal microscopy studies confirmed the potential of rG4s-C_8 complexes in the targeting of prostate cancer cells.

Overall, it is here demonstrated that the rG4 found in pre-miR-149 can be used as a cancer-selective delivery carrier of C_8 to prostate cancer cells.

1. Introduction

In recent years, the use of oligonucleotides as therapeutic agents has received the interest of researchers [1–3]. However, the efficacy of oligonucleotide-based therapies is highly impaired due to their susceptibility to degradation by nucleases and poor cellular internalization [4,5]. A way to potentially overcome these limitations is by using G-quadruplex (G4) structures. These structures are assembled through the interactions between four guanines that are organized in a cyclic Hoogsteen hydrogen-bonding arrangement [6], and have been shown to display favorable intrinsic features such as higher stability, higher resistance to nucleases and enhanced cellular uptake [7].

RNA G-quadruplexes (rG4s) are much more stable than DNA G4s. In addition to important structural advantages related to the thermodynamically stability and less hydration [8], the presence of the 2′-OH group of the ribose sugar locks the RNA in an anti-conformation, thereby favoring the parallel topology [9]. Consequently, rG4s have less topological diversity than DNA homologous [9]. Together, the high stability displayed by rG4s and the conserved parallel topology makes them very interesting molecules for drug development.

rG4s play an important regulatory role on a wide range of biological events and they are distributed in important regions of genome such as messenger RNAs (mRNAs) and non-coding RNAs [such as microRNAs (miRNAs)] [10]. In mRNAs, the presence of G4s mainly regulate the translation and the G4s found in non-coding RNAs have functional regulatory roles in pre- and post-transcriptional gene expression [10]. Taking this into account, several precursor microRNAs presenting G4 structures (pre-miRNAs-G4s) emerged as regulatory biologically relevant structures in RNA. The ability of pre-miR-149 [11], pre-miR-92b [12,13] and pre-miR-let-7e [14] to form G4 structures and regulate

* Corresponding author.
E-mail address: carlacruz@fcsaude.ubi.pt (C. Cruz).

https://doi.org/10.1016/j.ejpb.2019.07.017
Received 9 February 2019; Received in revised form 12 June 2019; Accepted 15 July 2019
Available online 17 July 2019

Dicer-maturation levels was recently studied. The presence of the G4 structure in pre-miRNAs has influence in miRNA biogenesis at the Dicer-maturation levels by competing with double-stranded stem-loop formation [13,15]. Under certain conditions, such as the presence of salts and/or ligands, the pre-miRNAs sequences can adopt the G4 structure avoiding the Dicer-mediated maturation and leading to sub expression of miRNA levels [11,13]. The G4 sequence 5′ GGGAGGGA GGGACGGG 3′ (rG4) found in pre-miR-149 was reported as a G4 parallel sequence [16]. Previously it was demonstrated that pre-miR-149 produces miR-149-5p and miR-149-3p, which act as antitumor miRNAs through the targeting of several oncogenic genes in several cancers, namely prostate cancer [17,18]. The rG4 sequence partially overlaps with miR-149-3p, a well-known tumor suppressive miRNA [11]. Sequences with the potential to form G4s are attractive NCL binders since NCL has high affinity to G4s [16] and is overexpressed in prostate cancer cells [19,20]. Recently, it was described that the loop length of G4 structures is a fundamental feature recognized by NCL [16,21]. Via binding to cell surface NCL, rG4 can gain intracellular access by endocytosis and benefit of NCL shuttling to the nucleus. Based on that, rG4 can bind NCL while carrying ligands for an intracellular targeted delivery with anticancer effect.

Acridine derivatives have been extensively studied due to its anticancer properties [22], namely BRACO-19 that is one of the most studied G4 ligands and the first to prove anticancer activity *in vivo* [23]. Recently the binding of acridine orange derivatives to DNA G4s has been reported using a variety of biophysical and biological experiments [22]. However, their potential to bind rG4s has not been yet unraveled.

Considering these evidences, we performed biophysical and biological studies to evaluate the formation and stabilization of rG4 found in pre-miR-149, and to assess the formation of its supramolecular complex with the acridine orange derivative C_8 and its precursor C_8-NH_2 (Fig. S1). A long loop rG4 sequence (5′-GGGAUUGGGAUUUUUGGGAUC GGG-3′) was also studied to assess the influence of loop length to NCL binding. The rG4s-C_8 complexes were evaluated in terms of *in vitro* stability, cellular uptake and localization, and cytotoxic activity to prostate cancer *versus* normal cell lines.

2. Materials and methods

2.1. Oligonucleotides and ligands

All oligonucleotides were obtained from Eurogentec (Belgium) or STAB VIDA Genomics (Portugal) with HPLC-grade purification. The rG4 sequences used are 5′-GGGAGGGAGGGACGGG-3′ with loop length 112 and 5′-GGGAUUGGGAUUUUUGGGAUCGGG-3′ with loop length 363. Stock solutions of approximately 1 mM were prepared using nuclease free water and stored at −80 °C until used. The concentration of oligonucleotide samples was determined from the absorbance at 260 nm by using the molar extinction coefficient. Annealing of oligonucleotide sequences was performed by heating the samples for 10 min at 95 °C and slowly cooling on ice for 30 min before the experiments. Synthesis and purification of C_8 and C_8-NH_2 ligands were performed as previously described [24]. Stock solutions of the compounds were prepared as 10 mM solutions in DMSO and their subsequent dilution was done using nuclease free water. Recombinant NCL peptide (partially RBD 2 and 3) was purchased from Cloud-Clone Corp. (Texas, USA). Stock solutions of approximately 1 mM were prepared using nuclease free water and stored at −80 °C.

2.2. Thermal difference spectroscopy (TDS) experiments

The TDS experiments were performed in an Evolution™ 220 UV/visible spectrophotometer (Thermo Scientific, USA). The TDS spectrum was obtained by subtracting the absorbance spectrum at 20 °C from the one at 90 °C. The spectrum at 90 °C was recorded after heating the sample at 90 °C for a few minutes, whereas the spectrum at 20 °C was recorded after annealing. TDS was carried out at 10 μM oligonucleotide strand concentration, in a lithium cacodylate buffer (10 mM) at pH 7.2, containing 0.1 or 5 mM KCl, using 1 cm path-length quartz cells. The UV TDS factors were determined according to the ratios ΔA240nm/ΔA295nm, ΔA255nm/ΔA295nm and ΔA275nm/ΔA295nm, where ΔAλ is the difference between the absorbance at 90 °C and at 20 °C at a given λ.

2.3. Circular dichroism spectroscopy

CD spectra were acquired in Jasco J-815 spectrometer (Jasco, USA), using a Peltier temperature controller (model CDF-426S/15). rG4s were annealed by heating at 95 °C for 10 min, following by slowly ice cooling in ice for 30 min. Otherwise stated, a 1 mm path-length quartz cuvette was used with an rG4 concentration of 10 μM in 10 mM lithium cacodylate at pH 7.2 containing 0.1 or 5 mM KCl. The required volume for the titrations was added directly in the quartz cell.

The CD melting experiments were performed in the temperature range 20–100 °C, with a heating rate of 2 °C/minute by monitoring the ellipticity at 263 nm. Spectra acquisition was performed in the absence and presence of 2 M equivalents of ligands. The ligands used were C_8 and C_8-NH_2. Data was converted into fraction folded (θ) plots using the following equation:

$$\theta = \frac{CD - CD_{\lambda}^{min}}{CD_{\lambda}^{max} - CD_{\lambda}^{min}} \quad (1)$$

where CD is the ellipticity of the monitored wavelength at each temperature and CD_{λ}^{min} and CD_{λ}^{max} are the lowest and highest ellipticity, respectively. Data points were then fitted to a Boltzmann distribution (OriginPro 2016) and the melting temperatures were determined from the two-state transition model using the first derivative method.

2.4. Fluorescence spectroscopy titrations

All steady-state fluorescence measurements were collected at 25 °C on a FluoroMax4 (Horiba, Japan) equipped with a Peltier-type temperature control system. Samples and references were scanned using 1 cm path length quartz microvolume cuvettes with an optimal volume of 700 μL. All spectra were scanned with an integration time of 0.5 s, an emission and excitation slit width of 2 nm and step size of 1 nm. The association between rG4 sequences and ligands/NCL was followed by titrating the oligonucleotides/NCL, respectively, and measuring the change in fluorescence. The titration was performed by adding previously annealed rG4 sequences or NCL stock solutions, followed by 3 min for equilibration. The obtained data was converted into fraction of bound ligand (α) plots using the following equation:

$$\alpha = \frac{I - I_{\lambda}^{free}}{I_{\lambda}^{bound} - I_{\lambda}^{free}} \quad (2)$$

where I is the fluorescence intensity of each ligand/rG4 or rG4/NCL ratio and I_{λ}^{free} and I_{λ}^{bound} are the fluorescence intensity of the free and fully bound ligand, respectively. Data points were then fitted to a hyperbolic function (OriginPro 2016) and K_D values were determined from the following saturation binding model.

$$\alpha = \frac{[rG4 \ \ or \ \ nucleolin]}{K_D + [rG4 \ \ or \ \ nucleolin]} \quad (3)$$

where α is the fraction of ligand bound and $[rG4 \ \ or \ \ nucleolin]$ is the oligonucleotide or NCL concentration. The saturation binding Hill slope model was used.

$$\alpha = \frac{[rG4 \ \ or \ \ nucleolin]^h}{K_D + [rG4 \ \ or \ \ nucleolin]^h} \quad (4)$$

where h is the Hill constant which describes cooperativity of ligand binding.

2.5. Viability/Proliferation assays

Human prostatic adenocarcinoma (PC-3) and human prostatic (PNT1A) cell lines were grown in Roswell Park Memorial Institute medium (RPMI) supplemented with 10% (m/v) fetal bovine serum (FBS), and 1% (m/v) penicillin-streptomycin. Cultures were maintained at 37 °C in a humidified atmosphere containing 5% CO_2. Cells were harvested, counted using the trypan blue exclusion method and seeded in 48-well plates (1×10^4 cells/well and 1×10^3 cells/well for compounds and rG4/rG4-C_8 complex, respectively) and after 24 h these were incubated with the compounds (C_8 and C_8-NH_2), rG4 or rG4-C_8 complex. The concentrations tested for the compounds ranged from 100 nM to 10 μM for incubation times of 12, 24, 48 and 72 h. The concentration used for rG4 and rG4-C_8 was 15 μM for an incubation time of 7 days. Wells containing untreated cells were used as a control. At the end of incubation, the media was replaced with fresh serum-free medium containing 3-(4,5-dimethylthiazol-2-yl)-2,5-diphenyltetrazolium bromide salt (MTT) and further incubated at 37 °C for 2 h. Finally, MTT containing medium was removed, formazan crystals were dissolved in DMSO and absorbance was recorded in a Bio-Rad xMark™ microplate reader (Bio-Rad, USA) at 570 nm. Cell viability data were expressed as mean ± SEM from at least three different experiments in comparison with untreated cells.

2.6. Nuclease stability assay

Nuclease stability assays of rG4 (20 μM) and rG4-C_8 complex were conducted firstly in RNase H solution (0.3-U/μL) (NZYtech, Portugal) and then in cell culture medium RPMI supplemented with 10% (m/v) FBS and 1% (m/v) penicillin-streptomycin for 1, 3, 12, 24 and 48 h at 37 °C. A stock solution of each sequence was prepared in 10 mM lithium cacodylate buffer and 0.1 mM KCl, pH 7.2. For nuclease stability assays a molar ratio of 1:1 of rG4:C_8 was prepared. Thereafter, rG4 and rG4–C_8 complex were annealed by heating to 95 °C for 10 min, following by a slowly cooling in ice for 30 min. 10 μL of each mixture was used for agarose gel electrophoresis, which was carried out using 1% agarose gel stained with 0.01% Green Safe in 1× TAE buffer (Tris-acetate-EDTA). The degradation patterns on the gel were visualized through UV light.

2.7. Confocal microscopy studies

PC-3 and PNT1A cell lines were grown in RPMI medium supplemented with 10% (v/v) FBS and 1% (v/v) penicillin-streptomycin. Cultures were maintained in a humidified chamber at 37 °C and 5% CO_2. The cell lines were subsequently harvested, counted using the trypan blue exclusion method and seeded in μ-Slide 8-well flat bottom imaging plates (Ibidi GmbH, Germany) at a plating density of 5×10^4 cells/well and incubated for cell attachment for 24 h at 37 °C and 5% CO_2. Thereafter, cells were incubated with the primary anti-NCL polyclonal antibody (Thermo Scientific, USA) for 2 h at 37 °C. Following primary antibody incubation, cells were washed 3× with fresh serum-free medium and incubated with secondary antibody anti-rabbit IgG conjugated with Alexa Fluor® 647 (Thermo Scientific, USA) for 1 h at 37 °C. Thereafter, cells were washed 3 × with fresh serum-free medium and stained with Hoechst 33342® nuclear probe (1 μM) for 10 min. Subsequently, the cells were incubated with C_8 (1 μM), rG4-Cy3.5 (1 μM) and rG4-C_8 complexes (1:1 ratio). Thereafter, the cells were transferred to a Zeiss LSM 710 confocal laser scanning microscope (CLSM; Carl Zeiss SMT Inc., USA) equipped with a plane-apochromat 63×/DIC objective and processed in Zeiss Zen (SP2, 2010), in order to evaluate the cellular uptake. The fluorescence images were obtained at 63× magnification.

3. Results and discussion

3.1. Binding and stabilization of the rG4s

The human precursor microRNA 149 (pre-miR-149) was identified by the SHALiPE approach, revealing the formation of a rG4 structure in this non-coding RNA with parallel topology, thermally stable, and conserved in mammals [11]. Herein, we studied the formation and topology of the rG4 found in pre-miR-149 (5′-GGGAGGGAGGGAC GGG-3′) by circular dichroism (CD) and UV/Vis spectroscopy, namely by the use of thermal difference spectroscopy (TDS). The TDS spectrum confirms that a G4 structure is adopted displaying two positive peaks at 245 and 275 nm and a negative peak at 295 nm (Fig. S2A) [25]. The TDS factors $\Delta A_{240}/\Delta A_{295}$, $\Delta A_{255}/\Delta A_{295}$, $\Delta A_{275}/\Delta A_{295}$ were determined and revealed values of 4.4, 7.1 and 3.8, respectively. These magnitudes are characteristic of a parallel G4 topology [26]. The CD spectrum shows typical CD signature of parallel G4 topology (Fig. S2B), with a positive peak at around 260 nm and a negative peak at around 240 nm. Altogether, these data show that the pre-miR-149 sequence adopts a parallel G4 structure in 0.1 mM KCl.

The stabilization through ligand binding is required to decrease the unfolded or partially folded intermediate states. The ligand C_8 was previously described as DNA intercalator [24] and DNA G4 binder/stabilizer of promoter and telomeric G4s with high affinity ($K_D \approx 10^{-7}\,M^{-1}$) and stabilizing ability ($\Delta T_m > 30\,°C$) [22]. Herein, we used a non-covalent strategy to associate the ligand C_8 and its precursor C_8-NH_2 with rG4s of pre-miR-149 in an attempt to bind and stabilize the G4 structure. The formation of stable complexes was assessed and characterized by CD and fluorescence spectroscopy. CD titrations were first performed to evaluate complex formation and/or structural modifications of the G4 structure upon ligand binding. The CD spectra of rG4 upon addition of C_8 and C_8-NH_2, showed no relevant variations on RNA ellipticity, suggesting an overall conservation of the parallel G4 topology (Fig. 1A and B).

The influence of ligands C_8 and C_8-NH_2 on the thermal stability of the rG4 was investigated by thermal denaturation using CD melting experiments. The ellipticity of parallel rG4 was monitored at 260 nm and distinct temperatures in the presence of KCl, allowing to determine the effect of the acridine orange derivatives in the melting temperature (T_m) of rG4 (51.8 ± 0.1) (Fig. 1C). In general, we observed that C_8 and C_8-NH_2 at 2 M equivalents led to an increase of more than 30 °C and 18.5 ± 0.4 in rG4 T_m, respectively.

The effect of the loop length in terms of rG4-C_8 complex formation and stability was also evaluated by TDS and CD experiments. The selected sequence was 5′-GGGAUUGGGAUUUUUGGGAUCGGG-3′ with loop length 363.

The TDS and CD spectra of the long loop showed that sequence adopts a parallel rG4 in presence of 5 mM KCl (Fig. S2C and D). The stabilization through C_8 and C_8-NH_2 at 2 M equivalents is similar to the obtained with the short loop, with $T_m > 30\,°C$ and 20.0 ± 0.5 °C for C_8 and C_8-NH_2, respectively (Fig. S3A, B and C).

3.2. Fluorescence binding studies with rG4 sequences

The binding strength of C_8 and C_8-NH_2 to rG4 sequences with loops 112 and 363 in the parallel conformation was investigated by fluorescence titrations. The fluorescence spectra of rG4 with loop 112 are presented in Fig. 2A and B and rG4 with loop 363 in Fig. S4A and B. The fraction of bound ligand (α) at each point of the titration was calculated following fluorescence changes at the maximum of intensity and was plotted as a function of the rG4 concentration to obtain an isotherm binding curve. The curve was fitted to a saturation binding model (Eq. (4), Section 2) and the apparent dissociation constants (K_D) were determined. The K_D values of rG4 with loop 112 with C_8 and C_8-NH_2 are 1.0 ± 0.1 μM and 0.9 ± 0.1 μM, respectively, and for rG4 with loop 363 are 0.8 ± 0.4 μM and 0.7 ± 0.1 μM, for C_8 and C_8-NH_2,

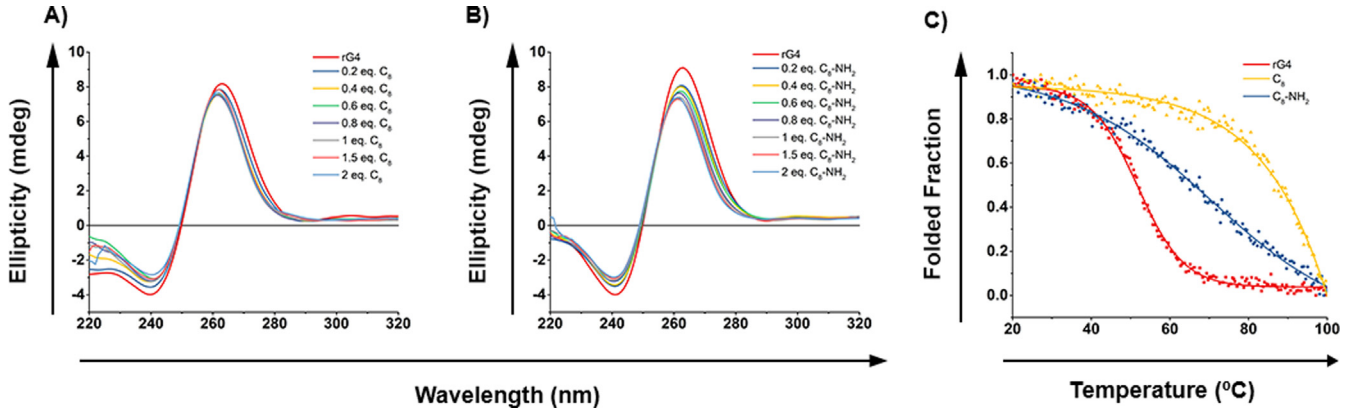

Fig. 1. CD titration spectra of short loop (112) rG4 at 10 μM with increasing concentrations of (A) C_8 and (B) C_8-NH_2. Spectra acquisitions were performed at 20 °C in 10 mM lithium cacodylate and 0.1 mM KCl; (C) CD melting curves at 10 μM in the absence and presence of 2 M equivalents of ligands in 10 mM lithium cacodylate and 0.1 mM KCl, respectively. Data points were recorded at 263 nm. Temperature corresponds to the temperature set by the Peltier system.

respectively. For both sequences the K_D values are in the low micromolar range, indicating high affinity, being similar to those previously reported for other G4 ligands, such as BRACO-19 [27] or pyridostatin [28].

3.3. Fluorescence binding studies with NCL

Then, we assessed the binding strength of NCL to rG4s (short and long loop rG4) and rG4s-C_8 complexes by fluorescence titrations. The fluorescence experiments were performed with rG4s labelled with Cy3.5. Fluorescence emission spectra of rG4s-Cy3.5 and rG4s-Cy3.5-C_8 complexes were recorded at 577 nm, in the absence and presence of increasing amounts of NCL RBD 2,3. The saturation binding plots were obtained by non-linear regression analysis and are presented in Fig. 3 and S5 for short and long loop sequences, respectively. The K_D values for the binding interaction between the short loop (112) rG4 and its rG4-C_8 complex with NCL were 309 ± 45 nM and 30 ± 22 nM, respectively. For the NCL interaction with the long loop (363) rG4 and its rG4-C_8 complex, the K_D values were 35 ± 14 nM and 2 ± 1 nM, respectively, indicating an increase in NCL binding upon loop extension. For both cases, the K_D values of complexes is in the low nanomolar range, in agreement with those previously reported for aptamer AS141, and thereby binds specifically to NCL [29]. This indicates that C_8 does not prevent the recognition of the NCL by the rG4.

3.4. Cytotoxic profile and antiproliferative effect of the complexes

The cytotoxicity effect of ligands C_8 and C_8-NH_2 in prostate cancer cell line PC-3 and an epithelial cell line derived from normal prostatic epithelium, PNT1A, was determined by the MTT assay. The results showed that the cytotoxicity of the C_8 and C_8-NH_2 increased with concentration and incubation time (Fig. S6). The relative cell viability of PC-3 and PNT1A cells, incubated for 72 h with free C_8 and C_8-NH_2 (Fig. S6), showed indistinct cytotoxic effect for these compounds. In fact, they induced a similar antiproliferative effect in PC-3 and PNT1A cells with IC_{50} values in the ranges 0.3–0.5 μM and 4.3–9.1 μM for C_8 and C_8-NH_2, respectively (Fig. S7). These IC_{50} values are lower than that obtained with G4 ligand BRACO-19 in DU145 cells after 96 h, with an IC_{50} value of 22.3 ± 0.8 μM [30]. In light of these results, we proceeded with the biological evaluation of C_8 that showed the highest antiproliferative activity and studied the possibility to enhance its cancer selectivity by exploring its supramolecular delivery by rG4 structures. Due to similar T_m and K_D values for long and short loop rG4 sequences, the antiproliferative effect of complex rG4-C_8 was evaluated only using short loop rG4 by MTT assay against PC-3 and PNT1A, to study if the supramolecular delivery strategy would lead to tumour-selective properties. The results are presented in Fig. 4. The rG4 showed reduced and similar cytotoxicity towards the PC-3 and the non-malignant PNT1A cells (75% mean viability). However, after mixing 15 μM rG4 with 1 μM C_8 to allow complex formation, the C_8 toxicity remained

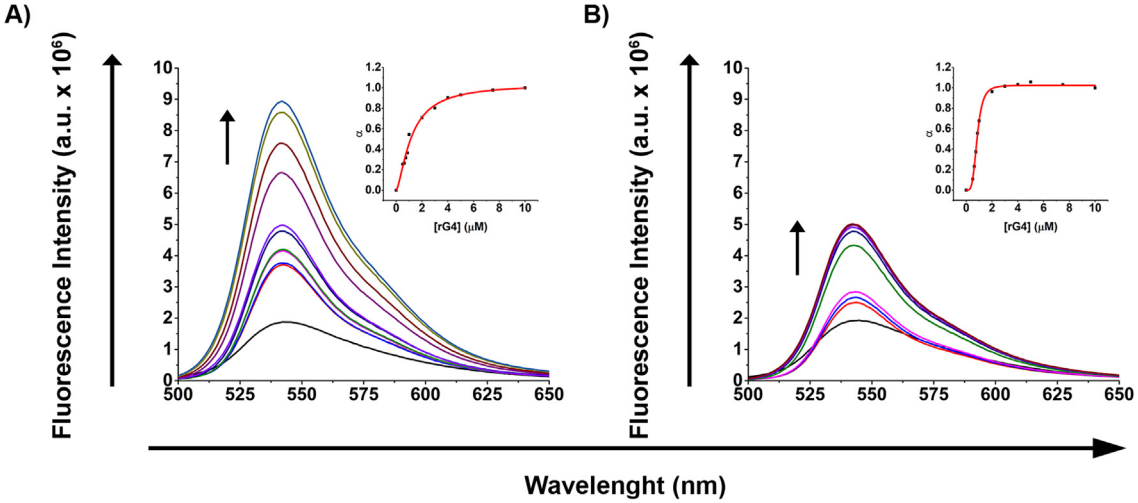

Fig. 2. Fluorescence emission spectra of (A) C_8 and (B) C_8-NH_2 at 5 μM with different concentrations of short loop (112) rG4 in 10 mM lithium cacodylate buffer and 0.1 mM KCl. Insets: fraction of ligand bound plots fitted to the saturation binding equation.

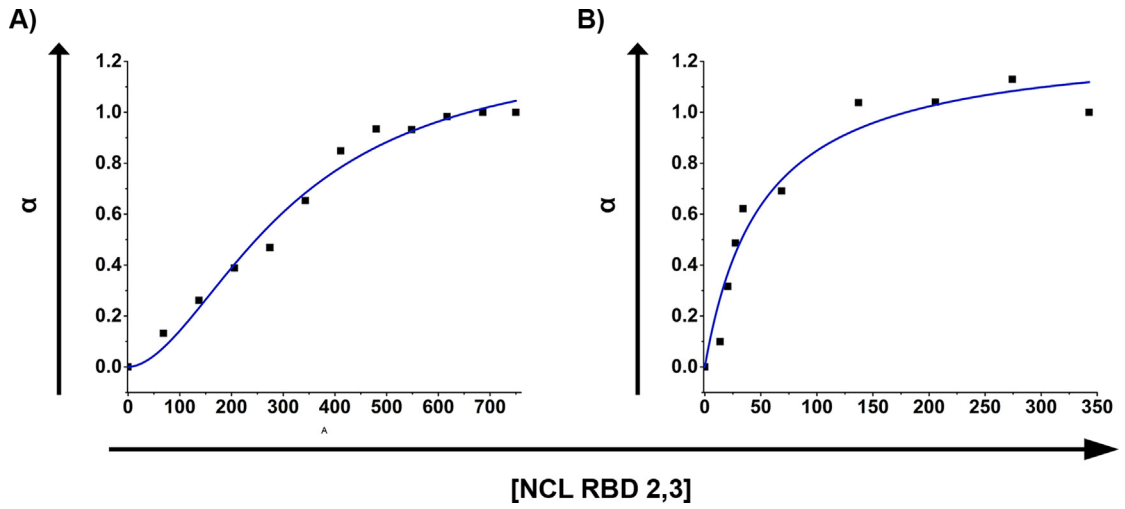

Fig. 3. Plots of the fraction of bound NCL to (A) short loop rG4-Cy3.5 and (B) short loop rG4-Cy3.5-C_8 complex at 1 μM in 10 mM lithium cacodylate buffer and 0.1 mM KCl.

quite pronounced against the PC-3 cells (25% mean viability) but was strongly reduced in the non-malignant cells (75% mean viability). This result suggests a cancer-selective antiproliferative effect of complex rG4-C_8. The lower cytotoxicity of C_8 towards non-malignant cells when complexed with rG4 may be due to the mechanism involved in the selective accumulation of oligonucleotides in cells. It has been proposed that DNA aptamer AS1411 is gradually cleared from normal cells by efflux or exocytosis 24–72 h post-treatment [31]. Additionally, normal cells have increased lysosomal activity in comparison with AS1411-treated cancer cells. Therefore, if the rG4-C_8 complex is capable of resisting cellular trafficking it may be cleared from normal cells by lysosomal degradation, thus promoting C_8 efflux and reducing its effects. In the case of PC-3 cells, the NCL-mediated disruption of rG4-C_8 trafficking and efflux might lead to C_8 entrapping inside the cancer cells [31].

3.5. Stability of rG4-C_8 complex

Since the rG4-C_8 complex (short loop rG4) exhibited a noteworthy antiproliferative activity, its resistance in biological environments was also evaluated through a degradation assay by incubation of the complexes, firstly with RNase H solution (0.3 U/μL) and then with culture medium supplemented with 10% FBS. Thus, the stability and resistance of the rG4 and rG4-C_8 complex were evaluated through gel agarose electrophoresis analysis (Fig. S8), after 1, 3, 12, 24 and 48 h of incubation, which is a crucial issue in its development as a potential therapeutic agent. The electrophoretic profile of rG4 and rG4-C_8 showed that both structures were completely resistant after 48 h in the presence of culture medium supplemented with 10% FBS. The electrophoretic profile of the rG4 in presence of RNase H (0.3 U/μL) showed the degradation of rG4. However, an increase in band intensities was observed when C_8 is complexed with rG4, suggesting a stabilizing effect of C_8.

We have also checked by CD spectroscopy during the 7 days if the rG4 parallel topology (Fig. S9A) was maintained in cellular medium and in the presence of C_8 (Fig. S9B). No significant changes in the ellipticity were noticeable in both cases.

3.6. In vitro cellular uptake and intracellular distribution of the rG4s-C_8 complex

The subcellular localization and cellular uptake of the rG4s-C_8

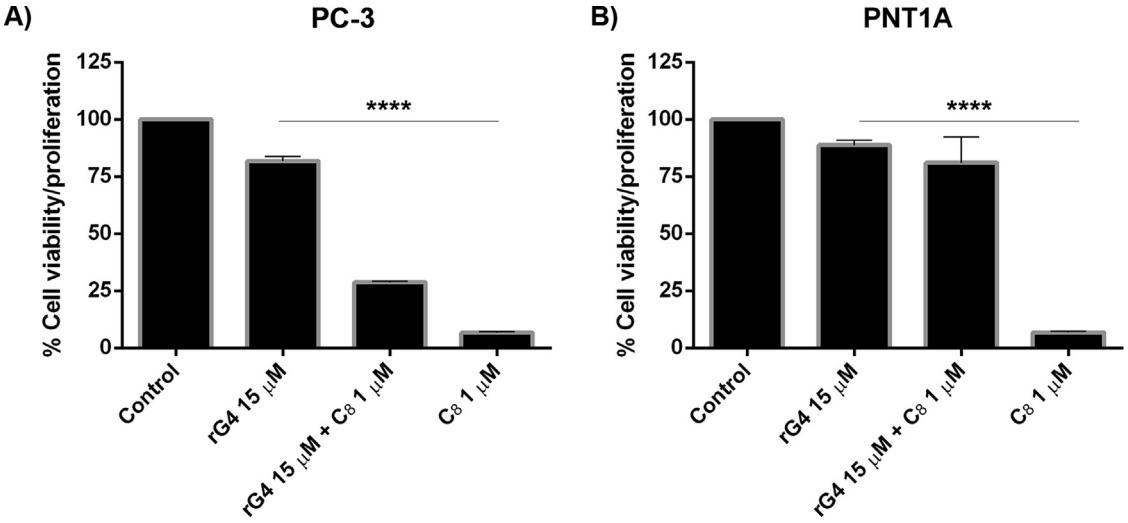

Fig. 4. Relative cell viability of (A) PC-3 and (B) PNT1A cell lines incubated for 7 days with short loop (112) rG4, and rG4-C_8 complex at C_8 and rG4 concentrations of 1 μM and 15 μM, respectively. Untreated cells were used as negative controls for cytotoxicity. Mean percentage values relative to untreated cells and standard error of the mean in 3 independent experiments are shown. The bars represent the mean and the lines represent the SEM associated. $^{****}P < 0.0001$ (one-way ANOVA).

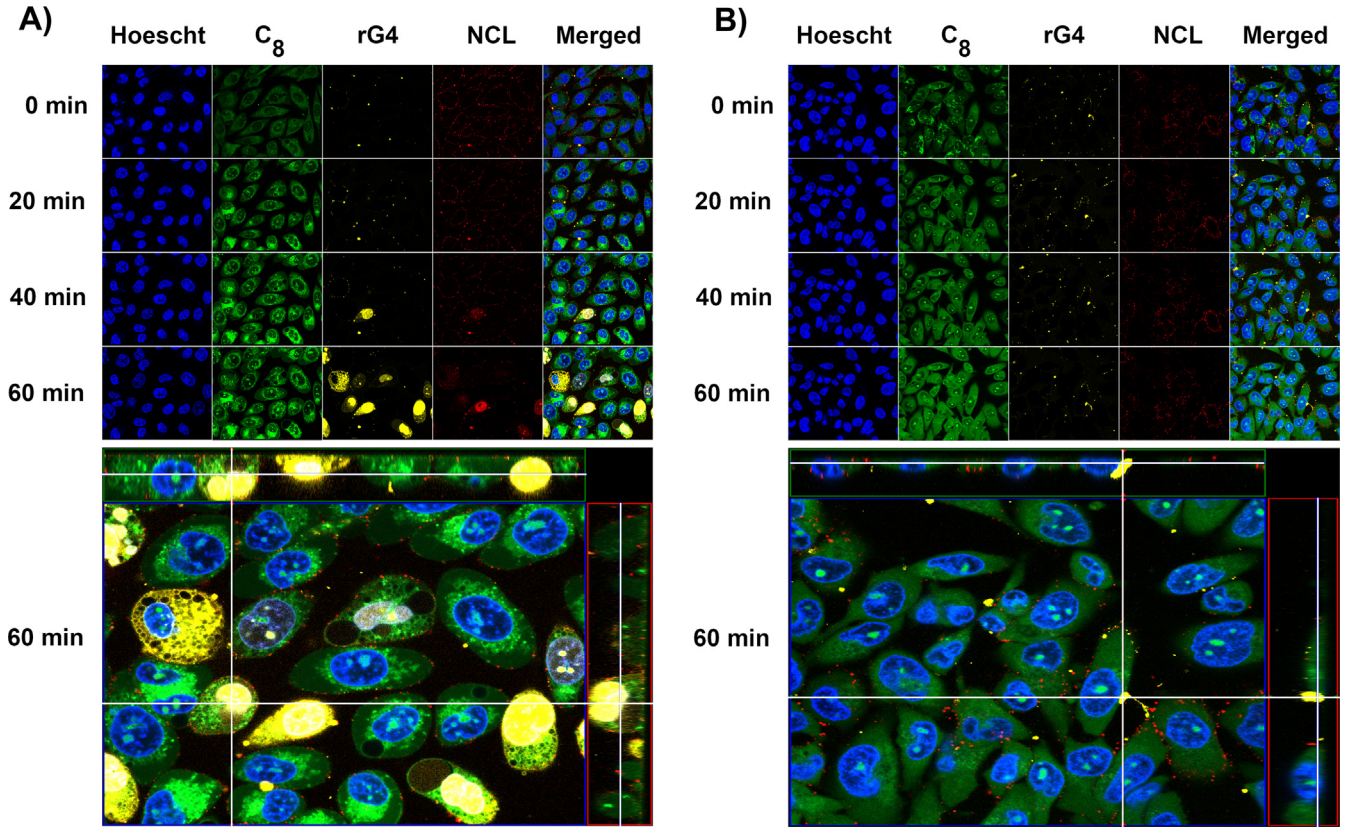

Fig. 5. Confocal laser scanning microscopy images showing the intracellular uptake of short loop rG4-C_8 complex from 0 to 60 min. For each panel, images showed the cells with nuclear staining by Hoechst 33342® (1 μM, blue); rG4 Cy3.5-C_8 complex (1:1 ratio, yellow); C_8 (1 μM, green); and NCL (red). NCL was labeled with the primary anti-NCL polyclonal antibody (1:100) and detected with the secondary antibody against IgG conjugated with Alexa Fluor® 647 (1:1000). (A) Representative z-stacks data showing PC-3 cell line and (B) Representative z-stacks data showing PNT1A cell line.

complexes (short and long loop rG4) in PC-3 and PNTA1 cells were evaluated by fluorescence confocal microscopy. We intend to evaluate if the loop length affects the uptake, intracellular distribution and NCL binding. The rG4s were labeled with Cy3.5 and, taking advantage of the intrinsic fluorescence of C_8, the distribution of the rG4s-C_8 complexes were visualized in the mentioned cell lines. The primary anti-NCL antibody conjugated with the secondary antibody AlexaFluor 647® was used to localize cell surface NCL. We have hypothesized that NCL is the cell surface target of rG4 and rG4-C_8 and may be a key transporter from the membrane through to the nucleus. As seen in Figs. 5 and S10, the complexes rG4-C_8 are able to penetrate cell membrane and localize in the cytoplasm of PC-3 cells. C_8 can be seen in the nucleoli in a free state which may suggest partial decomplexation and localization of the nucleolus as described for the ligand [22]. After 1 h of rG4-C_8 complexes incubation, changes in cell morphology consistent with the cytoplasmic vacuolation are observed, but less pronounced for long loop rG4-C_8 complex. The cytoplasmic vacuolation observed is similar to that seen for higher concentrations of the AS1411 in several cancer cells [32–34]. A more modest uptake of both rG4-C_8 complexes were detected in the cytoplasm of PNTA1 cells in agreement with the cytotoxic results (Fig. 5).

Overall, our study indicates that the rG4-C_8 complexes have tumour-selective properties, which are favourable features for its use as a potential cytotoxic agent [35]. Moreover, the observed cell specificity for PC-3 cells together with the enhanced antiproliferative activity exhibited by rG4-C_8 on cultured cells, in the absence of any transfection agent, suggest a mechanism of internalization mediated by NCL, which is more expressed in prostate cancer cells than in normal prostatic cells.

4. Conclusions

Herein, we have studied the rG4 found in pre-miR-149 as a drug delivery carrier of an acridine-based G4 ligand, C_8, with known anticancer properties. We demonstrated the formation of the rG4-C_8 complex, showing that C_8 has a high affinity to the rG4 and stabilizes the rG4 structure in more than 30 °C. We also evaluated a long loop of rG4 sequence and its C_8 complex in terms of stability and binding to NCL. Both rG4s-C_8 complexes bound NCL with high affinity ($K_D \approx 10^{-9}$ M), suggesting that C_8 complexation did not affect the recognition of NCL, which is necessary to obtain selective biological effects. Consistently, it was observed that rG4-C_8 has an augmented cytotoxic activity in PC-3 cells when compared with non-malignant cells.

The nuclease stability assay performed in biological conditions showed that the structure of rG4 and rG4-C_8 remain stable after incubation at 37 °C for 48 h in the presence of cell culture medium. This is a very favorable feature as many therapeutic oligonucleotides are highly unstable and thus easily degraded by nucleases.

Finally, the experiments performed with confocal microscopy indicated that complexes rG4s-C_8 internalized cancer cells and were partially maintained during cell internalization and trafficking to the nucleus; C_8 localized nucleoli in a free state which may suggest partial decomplexation.

Overall, the results suggest that rG4-C8 complex can be used for the development of delivery system to prostate cancer cells.

Acknowledgments

Tiago Santos acknowledges Fundação para a Ciência e Tecnologia (FCT), Portugal for the doctoral fellowship PD/BD/142851/2018 integrated in the Ph.D. Programme in NMR applied to chemistry,

materials and biosciences (PD/00065/2013). C. Cruz acknowledges the FCT project reference IF/00959/2015, FLAD-Healthcare 2020, Portugal project ref. 45/2018 entitled “Development of drug delivery nanocarrier for HPV infection”, MIT-EXPL/BIO/0008/2017 entitled “Biomedical device development based on pre-miRNA G-quadruplex” and UTAP-EXPL/NTec/0015/2017 entitled “DRug dElivery nAnosysteM for HPV infection therapy”. This work was also supported by the FCT project ref. UID/Multi/04349/2019 and by POCI – COMPETE 2020 – Operational Programme Competitiveness and Internationalisation in Axis I – Strengthening research, technological development and innovation (project POCI-01-0145-FEDER-007491).

Appendix A. Supplementary material

Supplementary data to this article can be found online at https://doi.org/10.1016/j.ejpb.2019.07.017.

References

[1] K.E. Lundin, O. Gissberg, C.I.E. Smith, Oligonucleotide therapies: the past and the present, Hum. Gene Ther. 26 (2015) 475–485, https://doi.org/10.1089/hum.2015.070.
[2] E.W.M. Ng, D.T. Shima, P. Calias, E.T. Cunningham Jr., D.R. Guyer, A.P. Adamis, Pegaptanib, a targeted anti-VEGF aptamer for ocular vascular disease, Nat. Rev. Drug Discov. 5 (2006) 123–132, https://doi.org/10.1038/nrd1955.
[3] N. Zhao, S.-N. Pei, J. Qi, Z. Zeng, S.P. Iyer, P. Lin, et al., Oligonucleotide aptamer-drug conjugates for targeted therapy of acute myeloid leukemia, Biomaterials 67 (2015) 42–51, https://doi.org/10.1016/j.biomaterials.2015.07.025.
[4] R. Juliano, M.R. Alam, V. Dixit, H. Kang, Mechanisms and strategies for effective delivery of antisense and siRNA oligonucleotides, Nucl. Acids Res. 36 (2008) 4158–4171, https://doi.org/10.1093/nar/gkn342.
[5] R.L. Juliano, The delivery of therapeutic oligonucleotides, Nucl. Acids Res. 44 (2016) 6518–6548, https://doi.org/10.1093/nar/gkw236.
[6] H. Huang, J. Zhang, S.E. Harvey, X. Hu, C. Cheng, RNA G-quadruplex secondary structure promotes alternative splicing via the RNA-binding protein hnRNPF, Genes Dev. 31 (2017) 2296–2309, https://doi.org/10.1101/gad.305862.117.
[7] P.J. Bates, D.A. Laber, D.M. Miller, S.D. Thomas, J.O. Trent, Discovery and development of the G-rich oligonucleotide AS1411 as a novel treatment for cancer, Exp. Mol. Pathol. 86 (2009) 151–164, https://doi.org/10.1016/j.yexmp.2009.01.004.
[8] A. Cammas, S. Millevoi, RNA G-quadruplexes: emerging mechanisms in disease, Nucl. Acids Res. 45 (2017) 1584–1595, https://doi.org/10.1093/nar/gkw1280.
[9] F. Zaccaria, Guerra C. Fonseca, RNA versus DNA G-quadruplex: the origin of increased stability, Chem. Eur. J. 24 (2018) 16315–16322, https://doi.org/10.1002/chem.201803530.
[10] M.M. Fay, S.M. Lyons, P. Ivanov, RNA G-quadruplexes in biology: principles and molecular mechanisms, J. Mol. Biol. 429 (2017) 2127–2147, https://doi.org/10.1016/j.jmb.2017.05.017.
[11] C.K. Kwok, A.B. Sahakyan, S. Balasubramanian, Structural analysis using SHALiPE to reveal RNA G-quadruplex formation in human precursor MicroRNA, Angew. Chem. Int. Ed. Engl. 55 (2016) 8958–8961, https://doi.org/10.1002/anie.201603562.
[12] G. Mirihana Arachchilage, P. Kharel, J. Reid, S. Basu, Targeting of G-quadruplex harboring pre-miRNA 92b by LNA rescues PTEN expression in NSCL cancer cells, ACS Chem. Biol. 13 (2018) 909–914, https://doi.org/10.1021/acschembio.7b00749.
[13] G. Mirihana Arachchilage, A.C. Dassanayake, S. Basu, A potassium ion-dependent RNA structural switch regulates human pre-miRNA 92b maturation, Chem. Biol. 22 (2015) 262–272, https://doi.org/10.1016/j.chembiol.2014.12.013.
[14] S. Pandey, P. Agarwala, G.G. Jayaraj, R. Gargallo, S. Maiti, The RNA stem-loop to G-quadruplex equilibrium controls mature MicroRNA production inside the cell, Biochemistry 54 (2015) 7067–7078, https://doi.org/10.1021/acs.biochem.5b00574.
[15] I.J. MacRae, K. Zhou, J.A. Doudna, Structural determinants of RNA recognition and cleavage by Dicer, Nat. Struct. Mol. Biol. 14 (2007) 934–940, https://doi.org/10.1038/nsmb1293.
[16] V. González, K. Guo, L. Hurley, D. Sun, Identification and characterization of nucleolin as a c-myc G-quadruplex-binding protein, J. Biol. Chem. 284 (2009) 23622–23635, https://doi.org/10.1074/jbc.M109.018028.
[17] A. Okato, T. Arai, Y. Yamada, S. Sugawara, K. Koshizuka, L. Fujimura, et al., Dual strands of pre-miR-149 inhibit cancer cell migration and invasion through targeting FOXM1 in renal cell carcinoma, Int. J. Mol. Sci. 18 (2017) 1969, https://doi.org/10.3390/ijms18091969.
[18] Y. He, D. Yu, L. Zhu, S. Zhong, J. Zhao, J. Tang, miR-149 in human cancer: a systemic review, J Cancer 9 (2018) 375–388, https://doi.org/10.7150/jca.21044.
[19] A. Tate, S. Isotani, M.J. Bradley, R.A. Sikes, R. Davis, L.W.K. Chung, et al., Met-independent hepatocyte growth factor-mediated regulation of cell adhesion in human prostate cancer cells, 197–197, BMC Cancer 6 (2006), https://doi.org/10.1186/1471-2407-6-197.
[20] A.G. Hovanessian, C. Soundaramourty, D.E. Khoury, I. Nondier, J. Svab, B. Krust, Surface expressed nucleolin is constantly induced in tumor cells to mediate calcium-dependent ligand internalization, PLoS ONE 5 (2010) e15787, https://doi.org/10.1371/journal.pone.0015787.
[21] S. Lago, E. Tosoni, M. Nadai, M. Palumbo, S.N. Richter, The cellular protein nucleolin preferentially binds long-looped G-quadruplex nucleic acids, Biochim. Biophys. Acta, Gen. Subj. 1861 (2017) 1371–1381, https://doi.org/10.1016/j.bbagen.2016.11.036.
[22] J. Carvalho, E. Pereira, J. Marquevielle, M.P.C. Campello, J.-L. Mergny, A. Paulo, et al., Fluorescent light-up acridine orange derivatives bind and stabilize KRAS-22RT G-quadruplex, Biochimie 144 (2018) 144–152, https://doi.org/10.1016/j.biochi.2017.11.004.
[23] A.M. Burger, F. Dai, C.M. Schultes, A.P. Reszka, M.J. Moore, J.A. Double, et al., The G-quadruplex-interactive molecule BRACO-19 inhibits tumor growth, consistent with telomere targeting and interference with telomerase function, Cancer Res. 65 (2005) 1489, https://doi.org/10.1158/0008-5472.CAN-04-2910.
[24] E. Pereira, L. do Quental, E. Palma, M.C. Oliveira, F. Mendes, P. Raposinho, et al., Evaluation of acridine orange derivatives as DNA-targeted radiopharmaceuticals for auger therapy: influence of the radionuclide and distance to DNA, Sci. Rep. 7 (2017) 42544, https://doi.org/10.1038/srep42544.
[25] J.-L. Mergny, J. Li, L. Lacroix, S. Amrane, J.B. Chaires, Thermal difference spectra: a specific signature for nucleic acid structures, e138–e138, Nucleic Acids Res. 33 (2005), https://doi.org/10.1093/nar/gni134.
[26] A.I. Karsisiotis, N.M. Hessari, E. Novellino, G.P. Spada, A. Randazzo, M. Webba da Silva, Topological characterization of nucleic acid G-quadruplexes by UV absorption and circular dichroism, Angew. Chem. Int. Ed. Engl. 50 (2011) 10645–10648, https://doi.org/10.1002/anie.201105193.
[27] S. Gilbert-Girard, A. Gravel, S. Artusi, S.N. Richter, N. Wallaschek, B.B. Kaufer, et al., Stabilization of telomere G-quadruplexes interferes with human herpesvirus 6A chromosomal integration, J. Virol. 91 (2017), https://doi.org/10.1128/JVI.00402-17.
[28] D. Koirala, S. Dhakal, B. Ashbridge, Y. Sannohe, R. Rodriguez, H. Sugiyama, et al., A single-molecule platform for investigation of interactions between G-quadruplexes and small-molecule ligands, Nat. Chem. 3 (2011) 782–787, https://doi.org/10.1038/nchem.1126.
[29] J.Y. Park, Y.L. Cho, J.R. Chae, S.H. Moon, W.G. Cho, Y.J. Choi, et al., Gemcitabine-incorporated G-quadruplex aptamer for targeted drug delivery into pancreas cancer, Mol. Ther. Nucleic Acids 12 (2018) 543–553, https://doi.org/10.1016/j.omtn.2018.06.003.
[30] C.M. Incles, C.M. Schultes, H. Kempski, H. Koehler, L.R. Kelland, S. Neidle, A G-quadruplex telomere targeting agent produces p16-associated senescence and chromosomal fusions in human prostate cancer cells, Mol. Cancer Ther. 3 (2004) 1201.
[31] P.J. Bates, E.M. Reyes-Reyes, M.T. Malik, E.M. Murphy, M.G. O'Toole, J.O. Trent, G-quadruplex oligonucleotide AS1411 as a cancer-targeting agent: uses and mechanisms, Biochim. Biophys. Acta, Gen. Subj. 1861 (2017) 1414–1428, https://doi.org/10.1016/j.bbagen.2016.12.015.
[32] Y.-A. Shieh, S.-J. Yang, M.-F. Wei, M.-J. Shieh, Aptamer-based tumor-targeted drug delivery for photodynamic therapy, ACS Nano 4 (2010) 1433–1442, https://doi.org/10.1021/nn901374b.
[33] J.S. Bishop, J.K. Guy-Caffey, J.O. Ojwang, S.R. Smith, M.E. Hogan, P.A. Cossum, et al., Intramolecular G-quartet motifs confer nuclease resistance to a potent anti-HIV oligonucleotide, J. Biol. Chem. 271 (1996) 5698–5703, https://doi.org/10.1074/jbc.271.10.5698.
[34] E.M. Reyes-Reyes, F.R. Šalipur, M. Shams, M.K. Forsthoefel, P.J. Bates, Mechanistic studies of anticancer aptamer AS1411 reveal a novel role for nucleolin in regulating Rac1 activation, Mol. Oncol. 9 (2015) 1392–1405, https://doi.org/10.1016/j.molonc.2015.03.012.
[35] T. Chang, C. Qi, J. Meng, N. Zhang, T. Bing, X. Yang, et al., General cell-binding activity of intramolecular G-quadruplexes with parallel structure, e62348–e62348, PLoS ONE 8 (2013), https://doi.org/10.1371/journal.pone.0062348.